

PACS numbers: 42.55.Px; 42.60.Mi; 42.65.Sf
DOI: 10.1070/QE2004v034n07ABEH002815

Dynamics of a delayed-feedback semiconductor laser depending on the number of stationary solutions

A.P. Napartovich, A.G. Sukharev

***Abstract*. The lasing regimes of a diode laser with an external mirror are studied using the Lang – Kobayashi (LK) equations in the limit of a small distance from the mirror. The system of LK equations is integrated directly with the help of a program package developed. In addition, the instability and bifurcation points of solutions are found by calculating numerically the contour integral and the spectrum of Lyapunov exponents is calculated. The hysteresis zones of the lasing dynamics are found, which appear when the phase of a reflected signal changes. The parameters are determined at which two or three attractors corresponding to different dynamic regimes coexist in the phase space. It is shown that, when the rest of parameters are fixed, an increase in the pump power leads to a chaotic regime according to a classical scenario via period-doubling bifurcations. The regions of parameters are found in which packets of regular pulsations are generated, and the transition of these packets to the chaotic regime is observed.**

Keywords: *semiconductor laser with an external mirror, radiation dynamics.*

1. Introduction

The lasing dynamics of a diode laser is often complicated and poorly reproducible. In the absence of control of the number of transverse modes, the spectrum of radiation pulsations contains characteristic frequencies of tens and hundreds of megahertz, and chaos, if it develops, is observed in time and space. If one transverse mode is stabilised, the nonlinearity of a medium in conjunction with the inhomogeneity of the laser field also can cause low-frequency pulsations of the field [1]. From the point of view of using chaotic signals for optical communications, a high frequency (more than 1 GHz) and good reproducibility of pulsation regimes are required. One of the variants providing both these conditions is the use of an additional mirror placed at a certain distance from a single-mode (in the transverse and longitudinal indices) diode laser. For the conditions when reflection from the external mirror is much weaker than from the semiconductor face, Lang and Kobayashi [2] derived dynamic equations, which are now widely used to study the dynamics of chaotic lasers.

The specific mathematical feature of the Lang – Kobayashi (LK) equations is related to the delay of the field reflected from the external mirror by the time τ_L, resulting in the appearance of a function with the retarded argument. The solution of equations with the retarded argument is unambiguously determined, strictly speaking, by the definition of functions on the interval $[-\tau_L, 0]$, which is equivalent to the appearance of an infinite number of degrees of freedom in the system. This circumstance, which makes such systems substantially different from more conventional laser systems with chaotic dynamics, has required the modification of mathematical methods for its study.

The author of paper [3] considered the problem of calculating the Lyapunov indices for an infinite-dimensional system, which characterise the dynamic stability of the system. The calculation procedure was proposed and the relation was found between these indices and different definitions of the fractal dimensionality related to the structure of integral curves in the phase space in the dynamic chaos regime. As follows from many calculations, the dimensionality of attractors, which are sets of the fractal (fractional) dimensionality embedded into the infinite-dimensional phase space, proves to be finite. By restricting the dimensionality of the phase space in calculations by a great number N, we can find the spectrum of Lyapunov indices (N values). If the positive indices, which indicate the dynamic instability of the system, change weakly with increasing N, we can assume that these indices have been found correctly. The question of the equivalence of the discrete system of equations, which is used in numerical calculations instead of differential equations, is solved by increasing the accuracy of calculations to achieve the convergence.

The system of the LK equations has five control parameters, and the radiation dynamics is still too complicated to be completely understood. In numerical calculations and experiments at different values of control parameters, nonlinear dynamic phenomena such as the period doubling [4], the quasi-periodic scenario of the transition to chaos [5], the Ikeda-scenario of the rearrangement of the system dynamics [6], and bifurcation cascades [7] were observed.

In Ref. [5], the evolution of the dynamic behaviour of solutions of the LK equations with increasing feedback

A.P. Napartovich, A.G. Sukharev State Scientific Center of the Russian Federation, Troitsk Institute for Innovation and Fusion Research, 142190 Troitsk, Moscow region, Russia;
tel.: (095) 334 04 50; e-mail: apn@triniti.ru; sure@triniti.ru

Received 29 December 2003; revision received 6 April 2004
Kvantovaya Elektronika **34** (7) 630 – 638 (2004)
Translated by M.N. Sapozhnikov

strength was studied at a long delay time. It was found that the limit cycle via the bifurcation was transformed to a quasi-periodic solution with two incommensurable frequencies, so that trajectories in the phase space cover a two-dimensional torus. Then, the third incommensurable frequency appears, generating a three-dimensional torus, which rapidly transforms to a chaotic attractor. As the feedback strength further increases, another chaotic attractor is created. Experiments [5] demonstrate that the lasing spectrum contains a set of frequencies corresponding to both attractors. If the time resolution is high enough, one can see that signals for different attractors are anti-correlated and a random switching from one attractor to another occurs.

When the frequency of relaxation oscillations is multiple of the delay time of the beam reflected from the external mirror placed at the distance L ($\nu_{ec} = c/2L$), the transition to chaos occurs via a chain of period doublings [4].

For a laser near the generation threshold with the round-trip transit frequency $\nu_{ec} = 1$ GHz, the transition to chaos via the cascade of bifurcations was found [7]. Stable lasing becomes unstable with increasing the feedback strength, passing through a series of Hopf bifurcations, and becomes chaotic. Then, rare deep holes in the laser power appear, which were related by authors [7] to low-frequency fluctuations (LFFs). As the feedback strength further increases, a stable lasing again appears, but at a different frequency and with a higher intensity. Then, the previous scenario repeats. The coexistence of two regimes – the LFF mode and stationary lasing, was experimentally observed.

In the papers considered above, which were devoted to the study of lasers with a long delay time of feedback, the frequency ν_{ro} of relaxation oscillations of the laser was used as a natural measure for the round-trip transit frequency ν_{ec}. For short resonators ($\nu_{ec} \gg \nu_{ro}$), the authors of paper [8] observed a regime in which laser generated a periodic train of regular pulsation packets (RPPs). Each packet consisted of light pulses with the pulse repetition rate ν_{ec}, while the RPP repetition rate was approximately an order of magnitude lower than the pulse repetition rate. In the case of a short delay, the dynamics of a laser with a delayed feedback proves to be similar to the dynamics of a pair of diodes with optical feedback without delay [9] and demonstrates a two-frequency (quasi-periodic) scenario of the transition to chaos.

The possibility of formation of a high-dimensional chaotic attractor with a high modulation frequency is of interest for cryptographic communication systems [10], by allowing the coding and transfer of a broadband signal (a bandwidth of 1.5 GHz has been already achieved).

It is well known that the LK equations have the so-called stationary solutions [11]. The number of different solutions and their stability depend on a combination of parameters, of which the most important are the feedback strength and delay time. In this paper, we made an attempt to relate the type of solutions to the number and stability of the so-called stationary solutions of the LK equations. The system of the LK equations was integrated directly with the help of a specially developed program packet (the Gear method adapted for problems with feedback). In addition, by calculating the contour integral, we found the instability points and bifurcations of solutions and, according to Ref. [3], calculated the spectrum of Lyapunov indices. We considered only relatively short delay times, which provide a high pulsation frequency.

2. Stationary solutions of the LK equations and their stability

Laser system with an external feedback have been extensively studied (the fundamentals of the theory and results obtained before 2000 can be found in Ref. [11]). The LK equations, describing a laser diode with an optical feedback, have, in the dimensionless variables, the form

$$\frac{\partial X}{\partial \tau} = (1 - \mathrm{i}R)NX(\tau) + \mathrm{i}MX(\tau - \tau_L)\exp(\mathrm{i}\varkappa), \tag{1}$$

$$\varkappa = \omega_0 \tau_L - \frac{\pi}{2},$$

$$T\frac{\partial N}{\partial \tau} = P - N - (1 + 2N)X^2, \tag{2}$$

where the equation for the complex field $X = E\exp(\mathrm{i}\varphi)$ can be split into the real equations

$$\frac{\partial E}{\partial \tau} = NE(\tau) - ME(\tau - \tau_L)\sin[\varkappa + \varphi(t - \tau_L) - \varphi], \tag{3}$$

$$\frac{\partial \varphi}{\partial \tau} = -RN + M\left[\frac{E(t - \tau_L)}{E(t)}\right]\cos[\varkappa + \varphi(t - \tau_L) - \varphi]. \tag{4}$$

Here, τ_L is the delay time in the feedback loop of length $2L$; ω_0 and E are the frequency and amplitude of the electromagnetic field. The gain in the active medium slightly above the lasing threshold can be approximately described by a linear function $G(\mathcal{N}) = 1/\tau_{ph} + g(\mathcal{N} - n_{th})$ of the carrier density $\mathcal{N}$, where $g = \partial G/\partial \mathcal{N}$ is the differential gain of the medium. The threshold gain is equal to the inverse lifetime τ_{ph} of a photon for a semiconductor laser without the external resonator. The dimensionless variables are defined as follows: the field amplitude is $X = (\frac{1}{2}g\tau_s)^{1/2}\mathscr{E}$ ($\mathscr{E}$ is the complex amplitude of a physical field); the inversion population measured with respect to the threshold is $N = \frac{1}{2}g\tau_{ph}(\mathcal{N} - \mathcal{N}_{th})$; and the normalised pump intensity is $P = \frac{1}{2}g\tau_{ph}(p\tau_s - \mathcal{N}_{th})$. The lifetime of carriers $T = \tau_s/\tau_{ph}$, the current time $\tau = t/\tau_{ph}$, and the strength of feedback from the external mirror $M = (R_c/R_d)^{1/2} \times (\tau_{ph}/\tau_d)$ (R_c and R_d are the reflectivities of the mirror and the diode facet, τ_d is the round-trip transit time in the diode) were normalised to the photon lifetime. The anti-waveguide parameter R is proportional to the ratio of the derivative of the refractive index with respect to population to the differential gain of the medium $R = -2k_0(\partial n/\partial \mathcal{N})(\partial G/\partial \mathcal{N})^{-1}$.

Equations (2)–(4) have the so-called stationary solutions [11], which are characterised by the nonzero frequency $\Omega = \partial\varphi/\partial\tau = \text{const}$, whereas $\partial E/\partial\tau = \partial N/\partial\tau = 0$. The stationary solutions can be found from the equations

$$\frac{N}{M} = \sin(\varkappa - \Omega\tau_L), \tag{5}$$

$$RN + \Omega = M\cos(\varkappa - \Omega\tau_L), \tag{6}$$

$$P = N + (1 + 2N)E^2. \tag{7}$$

From equations (5) and (6), the transcendent equation for the frequency Ω can be derived [11]:

$$\Omega = M\left(1+R^2\right)^{1/2}\sin\left[\Omega\tau_L - \varkappa + \arctan\frac{1}{R}\right]. \quad (8)$$

The number of solutions of this equation is determined by one parameter $s = M\tau_L(1+R^2)^{1/2}$, which is called the effective feedback strength [11]. The LK equations contain five external parameters: the pump excess over the threshold P, the lifetime T of carriers, the feedback delay time τ_L, the feedback amplitude M and phase $\varkappa$. The effective feedback strength s, which determines the number of stationary solutions, depends only on the product of two of them (we ignore the possibility of varying the value of R). Although the stationary solutions are formally dependent on time, the analysis of their stability with respect to small perturbations exponentially dependent on time [11] is reduced to the system of equations for variation of the coefficients corresponding to the population inversion n_{inv}, the field amplitude α and phase ψ:

$$\lambda\begin{pmatrix}\alpha\\ \psi\\ n_{\text{inv}}\end{pmatrix} = \begin{pmatrix} N(1-\mathrm{e}^{-\lambda\tau_L}) & ME(1-\mathrm{e}^{-\lambda\tau_L})\cos(\varkappa-\Omega\tau_L) & E\\ \left(-\frac{M}{E}\right)(1-\mathrm{e}^{-\lambda\tau_L})\cos(\varkappa-\Omega\tau_L) & N(1-\mathrm{e}^{-\lambda\tau_L}) & -R\\ \left(-\frac{2E}{T}\right)(1+2N) & 0 & -\gamma\end{pmatrix} \times\begin{pmatrix}\alpha\\ \psi\\ n_{\text{inv}}\end{pmatrix}, \quad (9)$$

where $\gamma T = (1+2P)/(1+2N)$.

The exponent λ can be found from the transcendent equation

$$g_3(\lambda) = (\gamma+\lambda)\{[M(1-\mathrm{e}^{-\lambda\tau_L})\sin(\varkappa-\Omega\tau_L) - \lambda]^2 + M^2(1-\mathrm{e}^{-\lambda\tau_L})^2\cos^2(\varkappa-\Omega\tau_L)\} - [2(P-N)/T] \times\{M(1-\mathrm{e}^{-\lambda\tau_L})[R\cos(\varkappa-\Omega\tau_L)+\sin(\varkappa-\Omega\tau_L)] - \lambda\} = 0. \quad (10)$$

The presence of the root $\lambda = 0$ is caused by an arbitrary choice of the phase reference point. The stability of stationary solutions is determined by the sign of the real part of λ. The solution is unstable when $\mathrm{Re}\lambda > 0$. To exclude the root at the coordinate origin, we introduce the function $g_2(\lambda) \equiv g_3(\lambda)/\lambda$.

Equation (10) takes the form

$$g_2(\lambda) = \lambda(\gamma+\lambda)\left[1+M^2f^2+2Mf\sin(\Omega\tau_L-\varkappa)\right] + \{2[P+M\sin(\Omega\tau_L-\varkappa)]/T\}\left\{1-Mf\left(1+R^2\right)^{1/2} \times\cos[\Omega\tau_L-\varkappa+\arctan(1/R)]\right\} = 0, \quad (11)$$

where $f = (1-\mathrm{e}^{-\lambda\tau_L})/\lambda$. The number of zeroes of equation (11) in the right complex half-plane can be expressed in terms of the contour integral covering the right half-plane,

$$\frac{1}{2\pi\mathrm{i}}\oint_{\mathrm{Re}\lambda>0}\mathrm{d}\lambda\,\frac{g_2'(\lambda)}{g_2(\lambda)}.$$

This contour integral can be reduced to the integral along the imaginary axis. Then, the number of zeroes of equation (11) in the right half-plane is determined by the expression

$$n = 1 - \frac{1}{2\pi\mathrm{i}}\int_{-\mathrm{i}\infty}^{\mathrm{i}\infty}\mathrm{d}\lambda\,\frac{g_2'(\lambda)}{g_2(\lambda)}.$$

This integral can be calculated numerically using one of the subroutines of the program packet. The instability develops when one of the zeroes of equation (11) passes from the left half-plane to the right one ($n = 1$). The Hopf bifurcation corresponds to the simultaneous crossing of the imaginary axis (symmetrically with respect to zero) by two roots. In this case, the lasing regime changes, and oscillations appear at the frequency coinciding with the imaginary part of the roots.

In the short resonator approximation, $M\tau_L \ll 1$, we can estimate the frequency of field oscillations at the Hopf bifurcation points. Assuming that $\lambda = \mathrm{i}\omega$, we obtain two complex conjugate roots with an accuracy to the second order in $\omega\tau_L \ll 1$:

$$\omega^2 = \frac{2(P-N)}{T} \times\frac{1-M\tau_L\left(1+R^2\right)^{1/2}\sin(\varkappa-\Omega\tau_L+\arctan R)}{1+M^2\tau_L^2-2M\tau_L\sin(\varkappa-\Omega\tau_L)}. \quad (12)$$

The critical value of the phase $\varkappa = \varkappa_{\text{cr}}$ can be found from the equation [assuming additionally that $M \ll P$ and taking equation (5) into account]

$$\frac{\gamma T}{P\tau_L} + 2M\tau_L[M\tau_L - \sin(\varkappa_{\text{cr}}-\Omega\tau_L)] + M\tau_L\left(1+R^2\right)^{1/2} \times\sin(\varkappa_{\text{cr}}-\Omega\tau_L+\arctan R) = 0. \quad (13)$$

In the rough approximation, the frequency of laser oscillations is of the order of the relaxation oscillation frequency $(2P/T)^{1/2}$. However, actually within the limits of applicability of expressions (12) and (13), the dependence of the oscillation frequency on the effective feedback strength s proves to be noticeable.

3. Calculation methods

The system of equations (2)–(4) was solved using one of the variants of the Gear method. The advantage of the Gear method over other multistep methods of the numerical integration of rigid systems is that this method allows one to change easily the integration step and order. The features of the calculation program used in the paper are described in Appendix I.

The spectrum of the Lyapunov exponents in systems with delay is calculated using the Packard–Takens procedure. According to the Takens theorem, it is necessary to use the embedded space with the dimensionality that is no less than two times plus unity greater than the dimensionality of the attractor being studied. Under this condition, it is expected that the spectrum of positive Lyapunov indices required for a finite system will be adequate to the spectrum for the initial infinite-dimensional system.

When the attractor dimensionality is small (in the case of a short external resonator), the dimensionality of the embedded space can coincide with the dimensionality n of the system. As the feedback delay time increases, the attractor dimensionality also increases. Then, the generalised Packard – Takens procedure [12] is used to construct a new embedded space of the dimensionality $m * n$, which is a combination of phase spaces formed by the state vectors of the system at the moments $i, i+1, \ldots, i+m-1$. It follows from the Takens theorem that almost for any realisations of the dynamic system constructed in such a way, its attractor will have the same properties as the required attractor if only the dimensionality of the constructed embedded space proves to be sufficient to describe the properties of the required attractor with the Hausdorff dimensionality d_{H} ($m * n \geqslant 2d_{\mathrm{H}} + 1$).

Under such a condition, the attractor dimensionality and the spectrum of Lyapunov indices found for a finite-dimensional space are good approximations of these quantities for the required attractor. For the LK equations, the number of equations is $n = 3$. It is natural to restrict the number m by the number of the grid nodes falling into the delay interval for the chosen integration step: $m = \tau/h$. The integration step is determined by the required accuracy, so that m proves to be proportional to the delay time. Already for $\tau = 10$, it is unreal to take the maximum value $m = 2000$ for calculations. However, there is no need to calculate many Lyapunov indices. When the index is equal to a great negative number, this dimension disappears (is compactified) for the attractor. Calculations showed that to find positive Lyapunov indices for $\tau = 80$, it is sufficient to take $m = 3 - 4$. The details of calculations of Lyapunov indices are presented in Appendix II.

4. Results of the numerical calculation of the system dynamics

It is convenient to analyse the solutions of the LK equations beginning from the frequency Ω of the stationary solution, which, for the fixed effective feedback strength, can be obtained as a function of the feedback phase $\varkappa$ (due to the obvious periodicity over $\varkappa$, it is sufficient to consider the region $0 < \varkappa < 360^\circ$). The greater is the effective feedback strength at the fixed phase, the greater is the number of stationary solutions. We analysed variations in the lasing dynamics with increasing the effective feedback strength accompanied by the complication of the dynamics. We paid main attention to the study of the role of the feedback phase, which is difficult to control in experiments. The presence of many parameters in the problem makes the classification of regimes and scenarios of the chaos development extremely complicated.

We used in numerical calculations the values $T = 1000$ and $R = 3$, which are typical for diode lasers. In addition, we considered only a laser pumped slightly above the threshold P. Figure 1 shows the dependence $\Omega(\varkappa)\tau_L/s$ for a comparatively weak effective feedback strength and the parameters $P = 0.2$, $M = 0.02$, and $\tau_L = 10$. On the curve the regions corresponding to stable stationary solutions are indicated, as well as the regions of instability with respect to Hopf bifurcations (the presence of two roots in the right half-plane). One can see that the instability to Hopf bifurcations is observed in a small vicinity of the phase $\varkappa = 90^\circ$. The first Lyapunov index at this point is $T\lambda_1 = 0$, which is

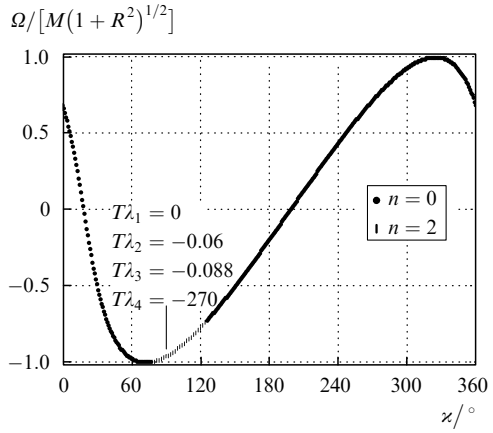

Figure 1. Stability diagram for stationary states for $P = 0.2$, $M = 0.02$, and $\tau_L = 10$; hereafter, n is the number of roots with $\mathrm{Re}\lambda > 0$.

explained by an arbitrary phase reference point. The next two indices are weakly negative: $T\lambda_2 = -0.06$ and $T\lambda_3 = -0.088$, whereas the fourth index is already a great negative number $T\lambda_4 = -270$. Therefore in this case, the embedded space is restricted by three dimensions.

Except the phase, all the quantities are strictly periodic in time (Figure 2 shows the behaviour of the field and inversion), which corresponds to the presence of the limit cycle in the phase space. The oscillation period is $T_{\mathrm{osc}} = 274$. The derivative of the phase (the instant frequency value) is also strictly periodic. However, the phase shift over the period is, as a rule, not multiple of 2π. The oscillation frequency near the lower bifurcation point $\varkappa \approx 80^\circ$ (Fig. 1) satisfies expression (12), and the position of the point can be found from expression (13).

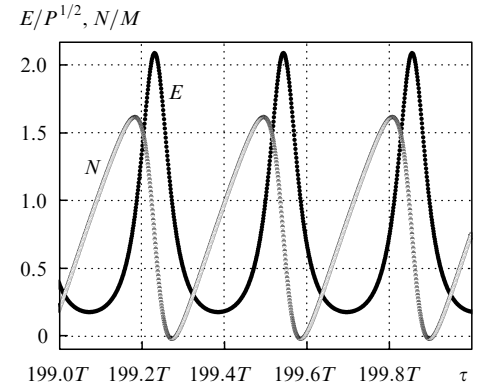

Figure 2. Time dependences of the field amplitude E and inversion N of the medium for $\varkappa = 90^\circ$, $P = 0.2$, $M = 0.02$, and $\tau_L = 10$.

As the feedback strength or delay time increases, the dependence $\Omega(\varkappa)\tau_L/s$ becomes ambiguous (Fig. 3), and the region appears where solutions are unstable (of the saddle point type) (the aperiodic development of instability). The interval where the Hopf instability is present increases noticeably. In the general case, if several stationary states correspond to one value of the phase, among which a stable state exists, the solution becomes, as a rule, stationary. Therefore, we paid the main attention in this work to the study of solutions near bifurcations and in the bistability

region. The shape of self-oscillations near the extreme bifurcation points is shown in Fig. 4, and the Lyapunov indices and oscillation periods are presented in Fig. 3. One can see from Fig. 4 that the type of pulsations strongly depends on the phase $\varkappa$, changing from incomplete modulation when the phase is small to separate intense peaks for the phase $\varkappa = 180^\circ$. Note that for $\varkappa = 30^\circ$, two Lyapunov indices are zero.

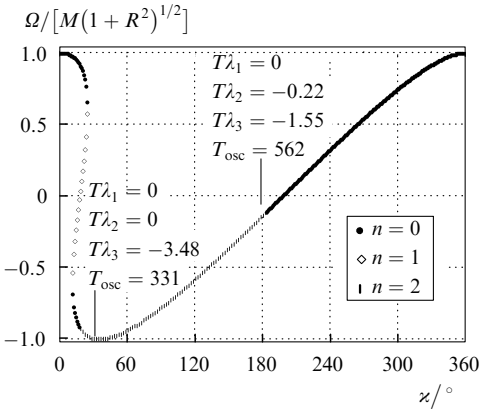

Figure 3. Stability diagram for stationary states for $P = 0.2$, $M = 0.02$, and $\tau_L = 20$.

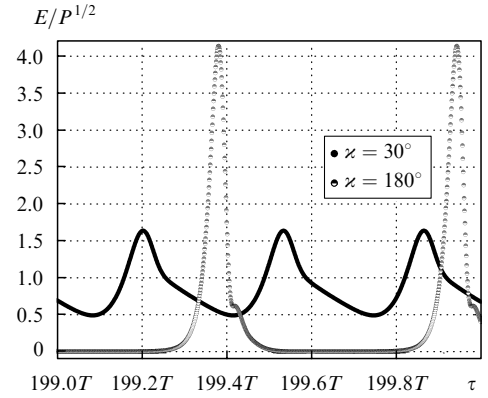

Figure 4. Dynamics of the field E for $\varkappa = 30$ and 180°, $P = 0.2$, $M = 0.02$, and $\tau_L = 20$.

The increase in the efficient feedback strength due to the increase in M up to 0.04 leads to the appearance of a region where two stable stationary solutions can coexist (Fig. 5). As a result, when the feedback phase changes, the hysteresis region appears where the solution depends on the direction of the phase variation (indicated by the dashed arrow in Fig. 5). In particular, as the phase decreases along the lower branch and comes to the bistability region, the stationary solution is stable until the jump to the upper stable stationary solution. As the phase increases from zero, the upper stationary solution is stable until the break (linear instability) indicated by the vertical arrow directed downward in Fig. 5. The development of instability leads to the spike regime with a deep modulation of the field and period $T_{\rm osc} = 819$, which is close to the inversion relaxation time ($T = 1000$). The hysteresis indicates the presence of two coexisting attractors in the phase space (a stable node and a limit cycle).

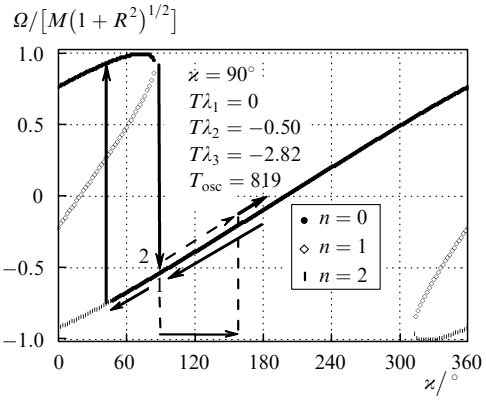

Figure 5. Stability diagram for stationary states for $P = 0.2$, $M = 0.02$, and $\tau_L = 20$. The straight arrow along the $\varkappa$ axis denotes the self-oscillation region.

Figure 6 shows the change in the stability regions of stationary solutions for the same efficient feedback but with different values of the feedback strength ($M = 0.02$) and delay time. In this case, the bistability region disappears, however, the hysteresis remains. As the phase increases from zero, the stationary solution is preserved until the break point 4, and then self-oscillations appear with the period $T_{\rm osc} = 529$ (Fig. 6, point 1; Fig. 7). Oscillations are preserved as the phase further increases up to $\varkappa \approx 185^\circ$ although the stationary solution is stable in this region. When the phase changes in the opposite direction, the stationary solution (Fig. 6, point 2) is preserved down to $\varkappa \approx 110^\circ$, and then self-oscillations appear, which have the form close to that observed at point 1. At $\varkappa \approx 70^\circ$, self-oscillations rapidly change to the upper stationary state. We found that, at the given parameters ($\varkappa \approx 120^\circ$, point 3), the system under study has one more attractor in the form of the limit cycle. This attractor was found when the phase rapidly changed from 165° to 120°. Therefore, for $\varkappa \approx 120^\circ$, depending on the initial conditions, one of the three regimes shown in Fig. 7 can be realised. The complicated nature of the system is demonstrated by the presence of the two zero Lyapunov indices for self-oscillation solutions. This example demonstrates the complexity of the phase space for the LK equations and the necessity of a search for new methods for its detailed study.

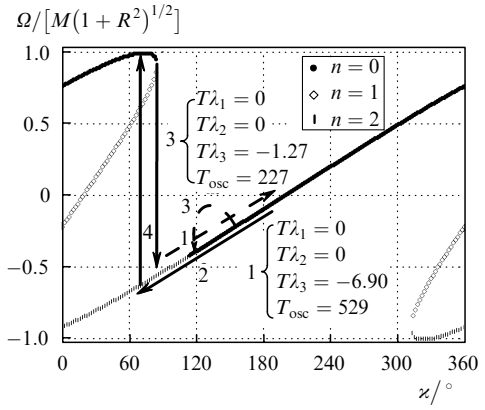

Figure 6. Stability diagram for stationary states for $P = 0.2$, $M = 0.02$, and $\tau_L = 40$. The dashed straight arrow denotes the hysteresis region with increasing $\varkappa$; 4 is the point of a break to a stationary state; bent arrow 3 shows the drop of $\varkappa$ used in calculations.

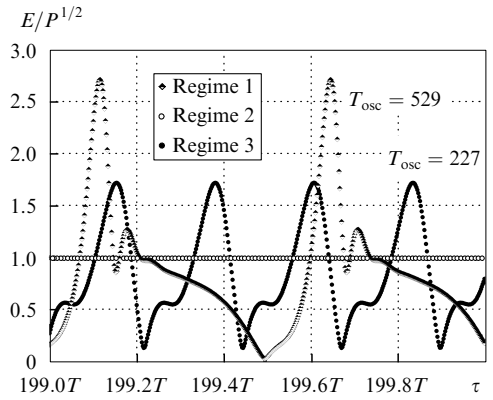

Figure 7. Dynamics of regimes 1, 2, and 3 for $\varkappa = 120^\circ$, $P = 0.2$, $M = 0.02$, and $\tau_L = 40$.

The efficient feedback strength was further increased also by two methods, either by increasing M (Fig. 8) or the delay time (Fig. 9). As before (cf. Fig. 5), as M increases, the bistability region broadens and the hysteresis is observed. Oscillations appearing after the Hopf bifurcation are close to harmonic oscillation with the period $1.9\tau_L$ ($\tau_L = 40$, Fig. 8) and $1.8\tau_L$ ($\tau_L = 80$, Fig. 9). This means that the dynamics is stabilised with increasing feedback strength: oscillations become weaker and the stability region of stationary solutions increases. As the delay time increases, the bistability region disappears (Fig. 9); however, the hysteresis is enhanced and the degree of modulation of oscillations increases.

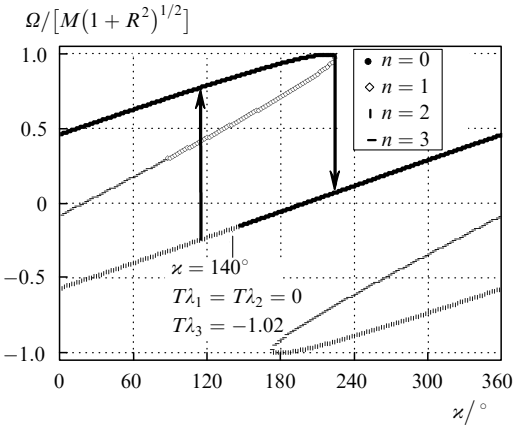

Figure 8. Stability diagram for stationary states for $P = 0.2$, $M = 0.04$, and $\tau_L = 40$. Jumps of regimes and the hysteresis region are shown by the arrows.

We studied the effect of the pump power level on the lasing dynamics for $M = 0.02$ and $\tau_L = 80$. For the same shape of the multiple-valued curve ($\Omega(\varkappa)\tau_L/s$), the increase in the pump power leads to the region broadening, where the stable stationary state is absent (cf. Fig. 9 and Fig. 10). When the phase is fixed, the increase in the pump power leads to a cascade of period doublings resulting in the development of the chaotic regime. The phase portrait of the chaotic solution for $\varkappa = 240^\circ$ and $P = 0.6$ is shown in Fig. 11. The first positive Lyapunov index for this regime is 5.05 and the next two indices are zero. In this case, the Lyapunov dimensionality is 3.7. Therefore, the increase in

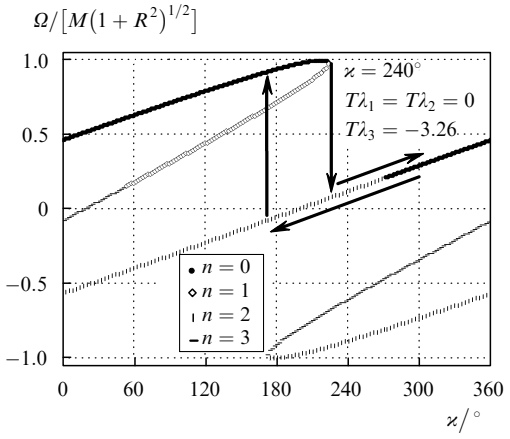

Figure 9. Stability diagram for stationary states for $P = 0.2$, $M = 0.02$, and $\tau_L = 80$.

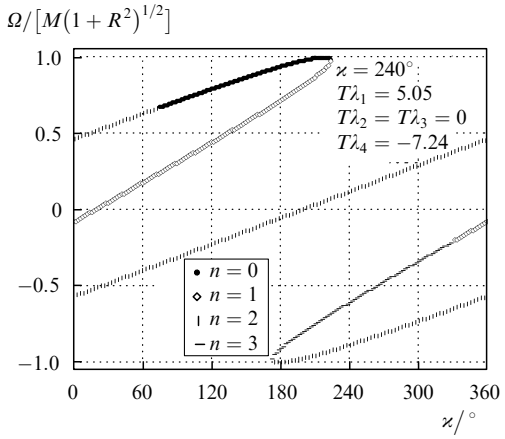

Figure 10. Stability diagram for stationary states for $P = 0.6$, $M = 0.02$, and $\tau_L = 80$.

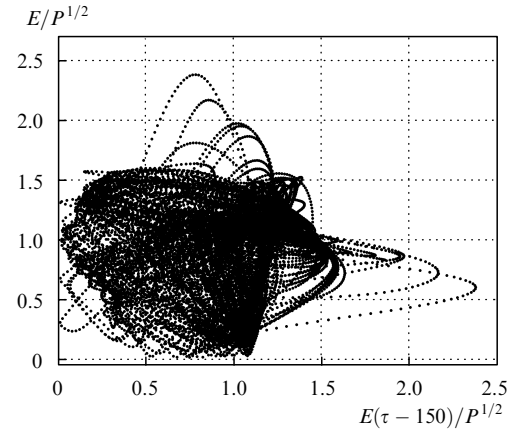

Figure 11. Phase portrait for the field amplitude in the chaotic regime for $P = 0.6$, $M = 0.02$, $\tau_L = 20$, and $\varkappa = 240^\circ$.

the pump power, as expected from the general considerations (the increase of nonlinearity) complicates lasing regimes.

The doubling of the delay time compared to that in Fig. 8 results in the increase in the number of possible stationary solutions (Fig. 12). However, almost all of them are unstable with respect to either linear perturbations or Hopf bifurcations. In the interval $\varkappa = 150^\circ - 240^\circ$, a stable

stationary solution cannot exist. Our calculations showed that during motion along the stationary state to lower phases, almost harmonic self-oscillations appear at the bifurcation point. Self-oscillations become more complicated only close to the boundary of stability of the upper branch of stationary states and take the form of packet of regular pulsations, described earlier [8]. For $\varkappa = 160^\circ$, the three Lyapunov indices are zero. In this case, the Lyapunov dimensionality is equal to three (see Appendix II), so that it is convenient to represent the phase space in the form of a three-dimensional torus.

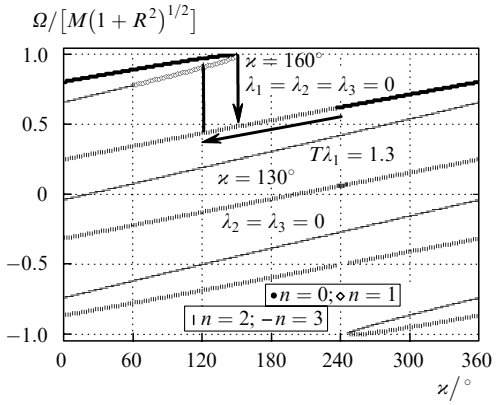

Figure 12. Stability diagram for stationary states for $P = 0.2$, $M = 0.04$, and $\tau_L = 80$. Jumps of regimes and the hysteresis region are shown by the arrows.

One can see from Fig. 13 that oscillations with the characteristic period $\sim 0.1T$ are modulated at a lower frequency. The scale of fast oscillations is determined by the frequency interval between the branches of stationary solutions, while the latter in turn are determined by the delay time τ_L. Indeed, the frequency interval in Fig. 12 is equal to $0.57M(1+R^2)^{1/2}$, corresponding to the period 87.4, which is close to the characteristic period of oscillations inside a packet. This allows us to interpret the system dynamics in terms of the three modes of an external resonator, each of them corresponding to the torus dimension in the phase space. The relaxation oscillation frequency $\omega = (2P/T)^{1/2}$ is estimated as 0.02 (period 314). Therefore, the period of a smooth RPP envelope is approximately equal to the doubled period of relaxation oscillations.

As the feedback phase further decreases (Fig. 12), the hysteresis is observed. Near the jump to the upper stationary solution ($\varkappa = 130^\circ$), the RPP regime passes to the dynamic chaos (the positive Lyapunov index appears) with rare deep holes in the field. As a whole, the lasing dynamics is close to the experimental dynamics observed in paper [7]. Note that the RPP regime and chaotic regime with deep rare holes are observed in a narrow interval of feedback phases. According to the Kaplan–Yorke formula (Appendix II), the dimensionality of the strange attractor in the chaotic regime is $d_L = 4.12$. The spectrum of Lyapunov indices contains one positive number and two zeroes: 1.3, 0, 0, −0.7, −5, −10.

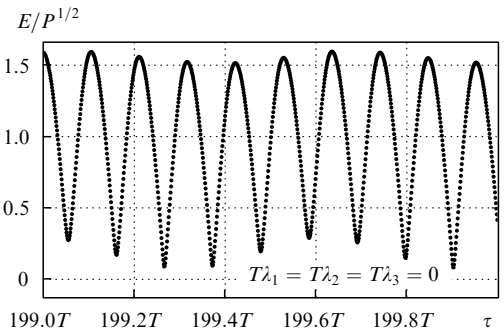

Figure 13. Field dynamics in the regime of packets of regular pulsations for $\varkappa = 160^\circ$, $P = 0.2$, $M = 0.04$, and $\tau_L = 80$.

5. Conclusions

We have studied different generation regimes of a diode laser with an external mirror using the LK equations based on the stationary solutions whose number increases with increasing the effective feedback strength. The system of the LK equations was integrated directly using a specially developed program package. In addition, we found numerically the instability and bifurcation points of solutions by calculating the contour integral and calculated the spectrum of Lyapunov indices following paper [3].

As the efficient feedback strength increases due to the feedback strength itself (the value of M), bistability regions appear, i.e., two stable stationary solutions for the same feedback phase. Simultaneously, the hysteresis appears with a more general behaviour, which is related to the presence of two coexisting attractors. When the effective feedback strength increases due to the delay time, the bistability region does not appear; however, the hysteresis remains. When the feedback phase was rapidly changed by a finite value, another self-oscillation regime appeared. As a result, we have shown that there exists the value of the feedback phase at which three attractors coexist (a stable node and two limit cycles).

As the pump power is increased, the rest of the parameters being fixed, the chaotic regime appears after the sequence of period-doubling bifurcations. The dimensionality of the strange attractor (3.7) is higher in this case than that for a couple pair of diode lasers [9]. A further increase of the feedback strength, when the delay time is $\tau_L = 80$ (in the units of the photon lifetime in laser diode resonator) leads to the appearance of packets of regular pulsations [8], which transfer to the characteristic chaotic regime with rare deep holes in the laser emission [7] when the feedback phase changes.

Acknowledgements. This work was supported by the Russian Foundation for Basic Research (Grant No. 01-02-16560) and a grant of the President of the Russian Federation (HSh-794.2003.2). The authors thank Laurent Larger (Franche-Comté University, France) for placing a copy of paper [3] at our disposal and Prof. Daan Lensra for a book 'Fundamental Issues of Nonlinear Laser Dynamics', as well as Prof. Bernd Krauskopf for useful critical comments.

Appendix I

Formulas for numerical integration

The numerical integration of the LK equations is based on the Gear method [13]. This method uses backward diffe-

rentiation for equations $y' = f(x, y)$; then, the prediction has the form

$$y_n = \sum_{i=1}^{k} A_i y_{n-i} + hB_1 f(x_{n-1}, y_{n-1}),$$

and the correction is

$$y_n = \sum_{i=1}^{k} a_i y_{n-i} + hb_0 f(x_n, y_n),$$

where A_i, B_1, a_i, and b_0 depend on the order k. The iteration process is performed using the transformation

$$y_n^{(v+1)} = y_n^{(v)} + b_0\left[hf\left(x_n, y_n^{(v)}\right) - hy_n'^{(v)}\right]. \tag{I.1}$$

Let us introduce the vectors Y_n and $Y_n^{(v)}$, the matrix D, and the Nordsic vector Z:

$$Y_n = \begin{pmatrix} y_n \\ hy_n' \\ y_{n-1} \\ y_{n-k+1} \end{pmatrix}, \qquad Y_n^{(v)} = \begin{pmatrix} y_n^{(v)} \\ hy_n'^{(v)} \\ y_{n-1} \\ y_{n-k+1} \end{pmatrix},$$

$$D = \begin{pmatrix} A_1 & B_1 & A_2 & A_k \\ \gamma_1 & \delta_1 & \gamma_2 & \gamma_k \\ 1 & 0 & 0 & 0 \\ 0 & 0 & 1 & 0 \end{pmatrix}, \quad Z(x_n) = \begin{pmatrix} y(x_n) \\ hy'(x_n) \\ (h^2/2)y''(x_n) \\ (h^3/6)y'''(x_n) \end{pmatrix}.$$

The prediction and iteration process for the vector Y_n are written as

$$Y_n^{(0)} = DY_{n-1}, \quad Y_n^{(v+1)} = Y_n^{(v)} + cF\left(Y_n^{(v)}\right), \tag{I.2}$$

where the residual function F and the vector c are

$$F\left(Y_n^{(v)}\right) = hf\left(x_n, y_n^{(v)}\right) - hy_n'^{(v)},$$
$$c = (\,b_0 \quad 1 \quad 0 \ldots \quad 0\,)^T. \tag{I.3}$$

In the Gear method, the Nordsic vector is used as the main vector, which is related to the vector Y_n by the transformation Q: $QY(x_n) = Z(x_n) + O(h^{k+1})$. Then, $Z_{n-1} = QY_{n-1}$ and

$$Z_n^{(0)} = QY_n^{(0)} = QDY_{n-1} = QD\left(Q^{-1}Q\right)Y_{n-1}$$
$$= \left(QDQ^{-1}\right)QY_{n-1} = \left(QDQ^{-1}\right)Z_{n-1}. \tag{I.4}$$

The matrix $P = QDQ^{-1}$ proves to be the triangular Pascal matrix. By introducing the vector $I = Qc = (\,l_0 \quad l_1 \quad l_2 \ldots \; l_k)^T$ containing the Gear coefficients, we obtain from (I.2)

$$Z_n^{(0)} = PZ_{n-1},$$
$$Z_n^{(v+1)} = QY_n^{(v+1)} = QY_n^{(v)} + QcF\left(Y_n^{(v)}\right) = Z_n^{(v)} + IF\left(Z_n^{(v)}\right), \tag{I.5}$$

because the residual function depends only on the first two components of the vector Y, while the transformation Q does not change the first two components. It is obvious that $Z_n = Z_n^{(0)} + Iw$, where

$$w = \lim_{v\to\infty} \sum_{j=0}^{v} F\left(Z_n^{(j)}\right),$$

and $F(Z_n) = 0$. Therefore, $F(Z_n^{(0)} + Iw) = 0$. We solve this equation by the Newton method:

$$w^{(v+1)} = w^{(v)} - \left[\frac{\partial F\left(Z_n^{(0)} + Iw^{(v)}\right)}{\partial Z} I\right]^{-1} F\left(Z_n^{(0)} + Iw^{(v)}\right),$$

which is equivalent to the procedure $Z^{(v+1)} = Z^{(v)} - IWF(Z_n^{(v)})$. The initial approximation is determined using (I.5), while the expression for the matrix W follows from the definition of the residual function (I.3)

$$W = \left[\frac{\partial F\left(Z_n^{(v)}\right)}{\partial Z} I\right]^{-1} = \left[hl_0 \frac{\partial f\left(x_n, y_n^{(v)}\right)}{\partial y} - l_1\right]^{-1}$$

and is related only to the Jacobian of the equation and the first two Gear coefficients. The final iteration process looks as

$$Z_n^{(0)} = PZ_{n-1}, \quad Z^{(v+1)} = Z^{(v)}$$
$$- I\left[hl_0 \frac{\partial f\left(x_n, y_n^{(v)}\right)}{\partial y} - l_1\right]^{-1}\left[hf\left(x_n, y_n^{(v)}\right) - hy_n'^{(v)}\right]. \tag{I.6}$$

Because the Nordsic vector consists of derivatives, the order is reduced by discarding the surplus components of this vector, while the increase in the order by unity is performed through the difference of the last components of two adjacent vectors Z_n and Z_{n-1}. The prediction of errors allows us to select the optimal step and order of the integration scheme. The algorithm was realised using the C++ language, and the feedback delay was taken into account by memorising the intermediate data in the form of the additional set of data.

Appendix II

Calculation of Lyapunov indices

Consider a system of nonlinear equations $\dot{x} = F(x, z)$, $z(t) = x(t - \tau)$, where $x(t)$ are the components of the vector depending on time. For the vector $y(t)$ of small perturbations with respect to the solution $x(t)$, determined by the initial conditions, the system of linear equations is written from the Jacobian of the initial system of equation on the solution trajectory

$$\dot{y} = \left(\frac{\partial F}{\partial x}\right)y + \left(\frac{\partial F}{\partial z}\right)y(t - \tau).$$

The solution of this equation is found at the integration step.

To solve the homogeneous part of the equation, we introduce the matrices

$$A_n(h) = \exp(G_n), \qquad G_n = \left(h\frac{\partial F}{\partial x}\right)_{t=(n+1/2)h},$$

which are defined at points in the middle of the integration intervals. This allows us to perform calculations to the second-order accuracy. The exponential $A_n(h)$ is calculated in the second order by expression $A_n(h) = (E - G_n/2)^{-1}\times$

$(E + G_n/2)$. For the inhomogeneous part of the equation, we define the second matrix as

$$B_n = \left(\frac{h}{2}\frac{\partial F}{\partial z}\right)_{t=(n+^1/_2)h}.$$

Then, the solution of the equation will be determined by the operator

$$y_{n+1} = A_n(h)\left[y_n + \frac{2}{h}\int_0^h A_n^{-1}(t')B_n y(t'-\tau)\mathrm{d}t'\right].$$

The solution is found by using the recurrence scheme

$$y_{n+1} = A_n[y_n + B_n y_{n-\tau/h}] + B_n y_{n+1-\tau/h},$$

$$y_{n+2} = A_{n+1}\left[y_{n+1} + \frac{4}{3}B_{n+1}y_{n+1-\tau/h} - \frac{1}{3}(A_n B_n y_{n-\tau/h} - B_n y_{n+1-\tau/h})\right] + \frac{2}{3}B_{n+1}y_{n+2-\tau/h}.$$

By dividing the integration axis into equal time intervals, for example, of duration τ, and by defining in terms of Q_i the expansion (contraction) transformation of the unit vectors $v_i^{(j)}$ on the ith time interval, we obtain $w_i^{(j)} = Q_i v_i^{(j)}$. A set of new vectors is orthogonalised by the Gramm–Schmidt method:

$$u_i^{(j)} = w_i^{(j)} - \sum_{k=1}^{j-1}(w_i^{(j)}, v_i^{(j)})v_i^{(j)},$$

where the unit vectors $v_i^{(j)}$ are constructed from the obtained orthogonal vectors $u_i^{(j)}$: $v_i^{(j)} = u_i^{(j)}/d_i^{(j)}$; here, $d_i^{(j)} = (u_i^{(j)}, u_i^{(j)})^{1/2}$ are vector lengths. Then, the Lyapunov indices are found as the limit of a sum over many time intervals

$$\lambda_j = \lim_{m\to\infty}(m\tau)^{-1}\sum_1^m d_i^{(j)}.$$

The so-called Lyapunov dimension d_L is determined from the spectrum of Lyapunov indices. If all the values of λ_j are ordered in their decreasing order $(\lambda_1 \geqslant \lambda_2 \geqslant \ldots \geqslant \lambda_n)$), then, according to the Kaplan–Yorke formula [12], we have

$$d_L = j + \sum_{i=1}^{j}\frac{\lambda_i}{|\lambda_{j+1}|},$$

where j is determined from the conditions $\lambda_1 + \lambda_2 + \ldots \lambda_j \geqslant 0$ and $\lambda_1 + \lambda_2 + \ldots \lambda_j + \lambda_{j+1} < 0$..

References

1. Bahert H.-Yu., Bogatov A.P., Eliseev P.G. *Kvantovaya Elektron.*, **5**, 603 (1978) [*Sov. J. Quantum Electron.*, **8**, 346 (1978)].
2. Lang R., Kobayashi K. *IEEE J. Quantum Electron.*, **16**, 347 (1980).
3. Farmer J.D. *Physica*, **4D**, 366 (1982).
4. Ye J., Li H., McInerney J.G. *Phys. Rev. A*, **47**, 2249 (1993).
5. Mørk J., Mark J., Tromborg B. *Phys. Rev. Lett.*, **65**, 1999 (1990).
6. Fischer I., Hess O., Elsäßer W., Göbel E. *Phys. Rev. Lett.*, **73**, 2188 (1994).
7. Hohl A., Gavrielides A. *Phys. Rev. Lett.*, **82**, 1148 (1999).
8. Heil T., Fischer I., Elsäßer W., Gavrielides A. *Phys. Rev. Lett.*, **87**, 243901 (2001).
9. Napartovich A.P., Sukharev A.G. *Kvanovaya Elektron.*, **31**, 147 (2001) [*Quantum Electron.*, **31**, 147 (2001)].
10. Ohtsubo J. *IEEE J. Quantum Electron.*, **38**, 1141 (2002).
11. Verduyn Lunel S.M., Krauskopf B., in *Fundamental Issues of Nonlinear Laser Dynamics*. Ed. by B. Krauskopf, D. Lenstra (Melville, NewYork: AIP Conference Proceeding, 2000) Vol. 548, p. 66.
12. Neimark Yu.I., Landa P.S. *Stokhasticheskie i khaoticheskie kolebaniya* (Stochastic and Chaotic Oscillations) (Moscow: Nauka, 1987).
13. Arushanyan O.B., Zaletkin S.F. *Chislennoe reshenie obyknovennykh differentsial'nykh uravnenii na fortrane* (Numerical Solution of Ordinary Differential Equations Using Fortran) (Moscow: Izd. Moscow State University, 1990).